2 August 2024

Indirect Detection of the Charm-Yukawa Interaction by analysing Higgs Boson production through the $H \rightarrow \gamma\gamma$ ATLAS measurements

Sienna Lam Chi-yin

Summary

I worked with Dr. Petar Bokan and Dr. Valentina Cairo to implement a likelihood fit on the ATLAS measurements of $H \rightarrow \gamma\gamma$. We analysed the effect of dependence of the Higgs boson production on the Charm-Yukawa interaction coupling strength, by observing the effects on the final state of Higgs boson production differential cross section as measured in $H \rightarrow \gamma\gamma$ analysis. By parameterising the Higgs boson production cross-section in terms of the Charm-Yukawa, Bottom-Yukawa and Top-Yukawa coupling strength, they can be varied to attempt to indirectly constrain the coupling strength of the Charm-Yukawa interaction relative to the coupling strength predicted by the Standard Model.

ATLAS Doc:	xxx-yyy-zzzz	
EDMS Id:	123456	
Version:	0.1	
Last modified:	`17:42 on 2 August 2024`	
Prepared by:	**Checked by:**	**Approved by:**
S. Lam	P. Bokan	V. Cairo

Contents

List of Figures

List of Tables

1 Introduction

The LHC, short for Large Hadron Collider, is a synchrotron which has a radius of 27 kilometers and a centre-of-mass energy of 13.6 TeV. It collides hadrons such as protons or ions in specific interaction points so that the collision products can be detected by various experiments, including ATLAS, ALICE, LHCb and CMS.

ATLAS, short for A Toroidal LHC Apparatus, is a general-purpose detector that along with CMS, studies phenomena of elementary particles predicted by the Standard Model, and it looks for particles beyond the Standard Model at the large energy scales. It is the largest experiment analysing the collisions in the LHC. The structure of ATLAS is shown in Figure 1. It measures the transverse momentum because the beams already possess longitudinal momentum along the beam axis, so the beam collisions possess an unknown initial longitudinal momentum meaning longitudinal momentum conservation cannot be accurately determined.

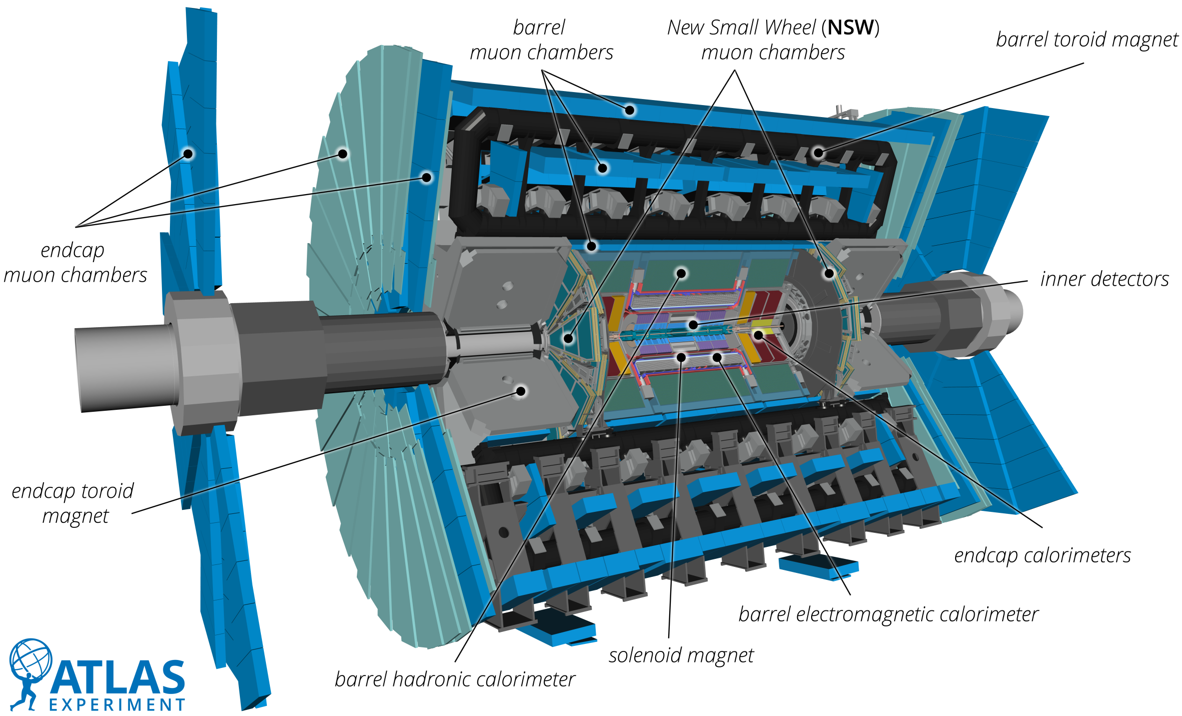

Figure 1: ATLAS has consists of 4 detectors: Inner Tracker, Electromagnetic Calorimeter, Hadronic Calorimeter and Muon Spectrometer. Bianchi and Collaboration [2022]

The first detector in ATLAS is the inner tracker which contains silicon pixel detectors and strip detectors (also known as semiconductor tracker) and transition radiation tracker. It detects the positions of charged particles as they pass through layers of pixels. There is also a magnet which bends the charged particle trajectory in a into a helical that is proportional to the particle momentum and charge.

Photons and electrons are detected in the Electromagnetic calorimeter which uses a Liquid Argon scintillator to measure their energy. Photons can only be detected with this

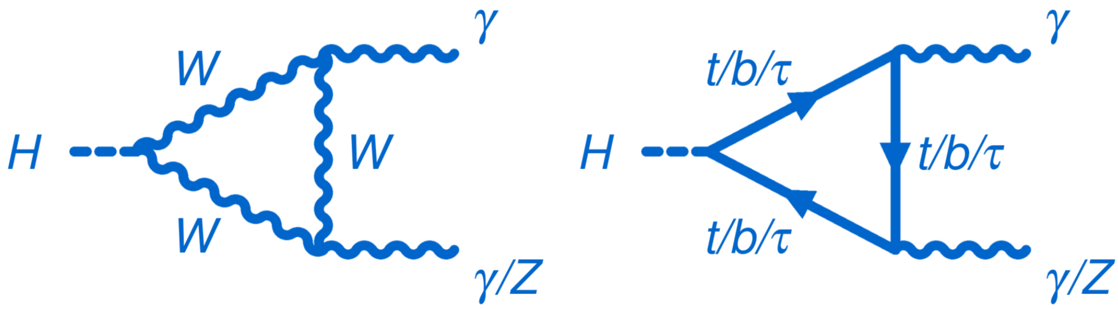

Figure 2: Higgs boson must produce a loop of massive particles, such as the W boson or heavy quarks, in order to decay into 2 photons. Collaboration [2022]

calorimeter because they are not charged so they do not interact with the inner tracker. The calorimeter contains lead absorbers and electrodes, held in place by a honeycomb structure. Each honeycomb section contains Liquid Argon as the active layer of the calorimeter. Wilkens and [on behalf ofthe ATLAS LArg Collaboration] When a photon collides with the lead, it undergoes an electromagnetic shower by emitting additional photons and decaying into positron-electron-pairs which ionise the Argon to produce a measurable current that is proportional to the energy.

There is also a Hadronic Calorimeter which detects measures the energy of hadrons, using many plates of plastic scintillators. Hadrons will form jets by emitting gluons, which then decay into more hadrons in a manner analogous to electromagnetic showers. The total energy in the shower is proportional to the energy of the initial hadron.

The last component is the Muon Spectrometer which has a large toroidal magnet to bend the trajectory of the muons so that the momentum can be determined from the curvature of the trajectory. The Muon Spectrometer is very large because the muon are very hard to bend with the magnet over short distances as they are very massive.

Photons can be detected with high resolution using the electromagnetic calorimeter because they have a clean final state. This is why the Higgs boson was first detected from $H \to \gamma\gamma$ production, even though they only have a branching ratio of 0.223% pb Collaboration [2022]. The reason that the branching ratio is low is because photons have no mass, so they only couple to the Higgs boson through production of an intermediary massive particle as shown in Figure 2.

2 Charm-Yukawa Coupling

The Higgs field is a scalar field which has a non-zero value in the vacuum. Excitations of this field will create Higgs boson particles with a mass of 125.09 GeV Collaboration [2023a] that can interact directly with all massive particles.

The Standard Model predicts that interactions between fermions and the Higgs boson are proportional to the fermion's mass, but for interactions between the Higgs boson and other bosons it is proportional to the square of the boson's mass.

The coupling strength for the Top-Yukawa, Bottom-Yukawa and Tau-Yukawa interactions have been precisely determined, but the Charm-Yukawa interaction is quite hard to measure. Currently, direct measurements of $H \to c\bar{c}$ only yield a constraint on the coupling modifier of $|\kappa_c| < 4.2$ ATLAS [2024], where $\kappa_c = \frac{y_c}{y_c^{SM}}$ where y_c is the coupling strength. One of the reasons is because the $H \to c\bar{c}$ decay is rare, because the charm quark is very light at only 1.27 GeV. This causes the $H \to c\bar{c}$ to have a branching ratio of around 2.884% Collaboration [2022] as calculated in the Standard Model. In addition, charm-initiated quark jets are difficult to distinguish from other quark or gluon jets. Charm quarks are also produced in many other processes when 2 protons are collided, such as the $Z \to c\bar{c}$ decay, which means that the background rates for $H \to c\bar{c}$ are very high.

As an alternative, indirect detection method can be used, by measuring the effect of the Charm-Yukawa interaction on Higgs boson production. The Charm-Yukawa interaction affects Higgs boson production because some of the production modes directly depend on it, with the cross section given by the Equation 1. In this equation, the Standard Model predicted cross sections for all major production modes are scaled by multiplying them directly with the coupling modifiers if they depend on Charm-Yukawa, Bottom-Yukawa and Top-Yukawa interactions respectively Bokan et al. [2022]:

$$\begin{aligned}\sigma_{pp\to H} = \kappa_t^2(\sigma_{ggF}^{tt} + \sigma_{ttH}) + \kappa_t\kappa_b\sigma_{ggF}^{tb} + \kappa_c\kappa_t\sigma_{ggF}^{ct} + \kappa_b\kappa_c\sigma_{ggF}^{bc} \\ + \kappa_b^2(\sigma_{ggF}^{b} + \sigma_{b\bar{b}\to H}) + \kappa_t^2(\sigma_{ggF}^{t} + \sigma_{t\bar{t}\to H}) + \sigma_{other}\end{aligned} \quad (1)$$

The Charm quark is involved in Higgs boson production in 2 ways. The first is gluon-gluon Fusion, where 2 gluons form a loop of Charm Quarks which allows them to combine into the Higgs boson, as shown in Figure 3. The loop of charm quarks also interferes with the loops of Top and Bottom quarks, overall having a combined impact on the Higgs boson production cross section.

The second is Quark-Quark Fusion, where a Charm quark and a Charm antiquark annihilate to produce a Higgs boson, as shown in Figure 4. This requires the two particles to have a total centre-of-mass energy greater than the Higgs boson mass-energy of 125.09 GeV.

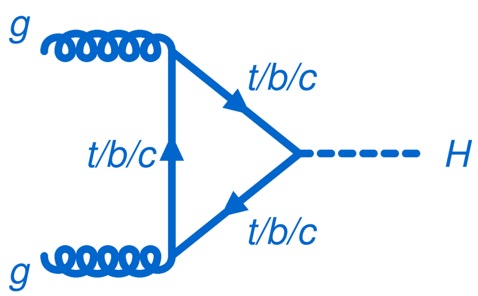

Figure 3: Gluon-gluon Fusion process, where the fermion propagators are either Top, Bottom or Charm quarks. Because the initial and final states of gluon-gluon Fusion are the same, different quark flavours can interfere Collaboration [2022].

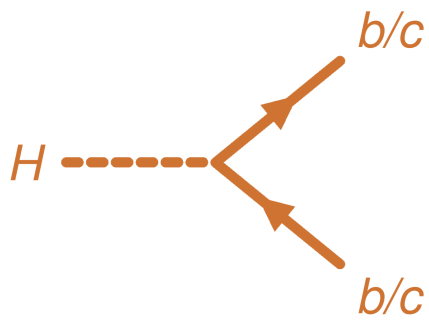

Figure 4: Higgs boson decays into a quark-antiquark pair, which could be either Bottom or Charm quarks. The diagram can also be read from right to left, as the fusion of a quark-antiquark pair to produce a Higgs boson Collaboration [2022].

The Standard Model predicts the contributions of each term for the parameterised cross section given in Equation 1. Using the predicted SM values for the contributions to the differential cross-section as a function of Higgs boson transverse momentum, and then dividing the cross-sections by the momentum width of each bin, we can produce a graph that shows the contribution of each term to the total differential cross-section, as shown in Figure 5:

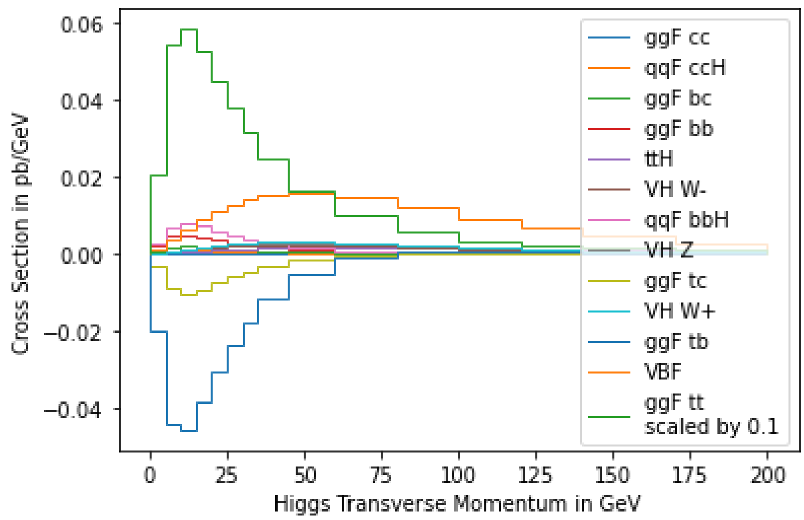

Figure 5: Differential cross section of the Higgs boson production modes. ggF refers to Gluon-Gluon Fusion, qqF refers to Quark-Quark Fusion, ttH is $gg \to ttH$, VBF is Vector Boson Fusion $qq \to VV \to H$, and VH is direct Higgs Boson production from a single Vector boson as follows $qq \to V \to VH$.

As the graph shows, the Top-Top gluon-gluon fusion term has the largest contribution

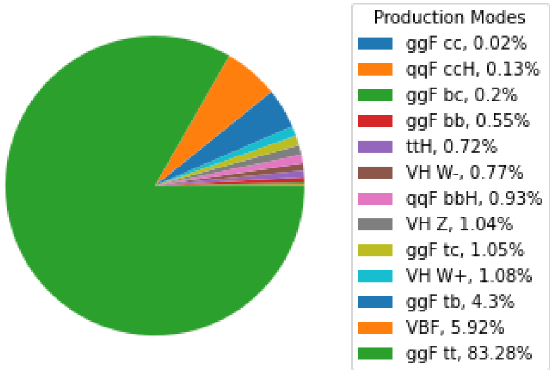

Figure 6: Piechart showing the relative contribution of each production mode to the Higgs boson production, including interference terms in Gluon-Gluon Fusion. The legend is sorted from smallest to largest in terms of absolute value of the contributions to the cross-section, which was also used to sort the legend for Figure 5.

by far, so it is scaled by a factor of 0.1 to make the other contributions more visible. This is because Top quark mass (172.52 ± 0.33 GeV) Collaboration and Collaboration [2024] is larger than Bottom quark mass ($4.18^{0.03}_{-0.02}$ GeV) Workman et al. [2022] and Charm quark mass (1.27 ± 0.02 GeV) Workman et al. [2022], so the top quarks couple most strongly to the Higgs boson.

The terms can be sorted by their contribution to the cross-section, using the Riemann sum of the step-like curves, to find the area under each curve. This reveals the predominance of Top-Top Gluon-Gluon Fusion, Vector boson Fusion and Top-Bottom Gluon-Gluon Fusion interference over all other terms, as shown in Figure 6.

Visualising the effect of varying the κ_c and κ_b coupling modifiers on the Higgs boson production cross-section, the predicted differential cross-sections for a predefined set of transverse momentum bins was plotted using the post-fit parameterised model. As shown in Figure 7, it becomes clear that when increasing κ_c or κ_b, the peak of the Higgs boson production differential cross-section increases, while the shape remains similar. However, when κ_c or κ_b are negative, the shape of the differential cross-section changes because the cross-section in the higher momentum bins is suppressed while the cross-section in the lower momentum bins is enhanced.

3 Statistical Analysis

A statistical analysis of the Higgs boson production differential cross-section Collaboration [2023b] to fit the parameters in Equation 1 to the ATLAS data. The fit is used to statistically infer the constraints on the coupling modifiers such as κ_c

We use a multivariate Gaussian Likelihood, which takes the form of the Equation 2 as shown below:

$$L(\vec{\sigma}(\vec{\kappa}, \vec{\theta})|\vec{x}, \boldsymbol{V}) = e^{\left(-\frac{1}{2}(\vec{x}-\vec{\sigma})^T \boldsymbol{V}^{-1}(\vec{x}-\vec{\sigma})\right)} \times \prod_j \text{Gauss}(\theta_j; 0, 1) \tag{2}$$

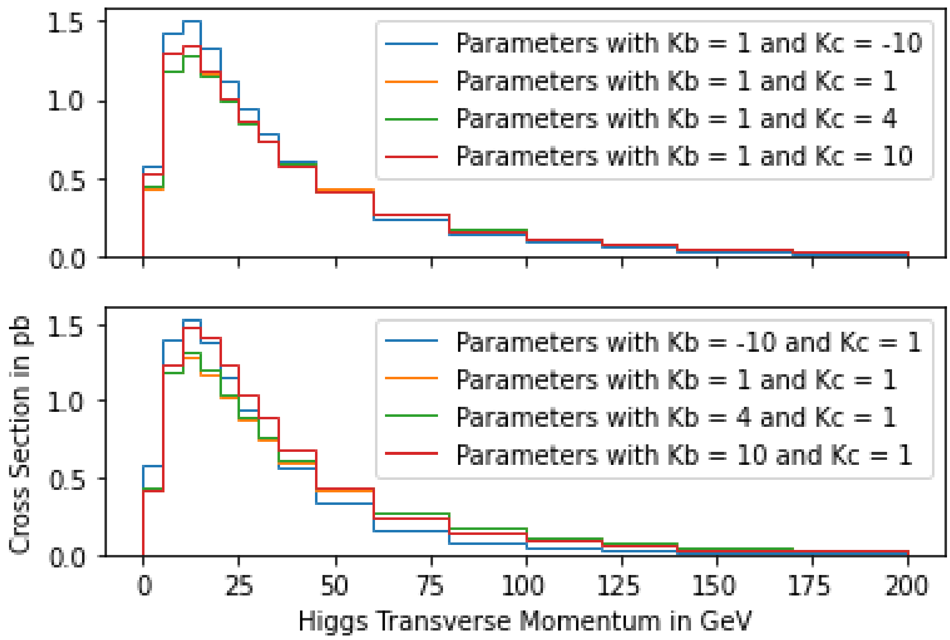

Figure 7: Change in the differential cross section for a few different parameters

The vector $\vec{x}$ is a list of all of the ATLAS measurements, and $\boldsymbol{V}$ is the covariant matrix of these measurements. $\vec{\sigma}$ is a list of all the parameters including the parameters of interest ($\vec{\kappa}$), and the nuisance parameters ($\vec{\theta}$). The Gauss($\theta_j; 0, 1$) term represents a Gaussian constraint on the values of the nuisance parameter θ_j between 0 and 1. In this context, the nuisance parameters represent the systematic uncertainties of the ATLAS experiment. These include the calculation and resummation uncertainties, QCD scale uncertainty, uncertainties in Parton Distribution Function and uncertainties in Parton Shower model Collaboration [2023b]. They modify the cross-section using the Equation 3:

$$\sigma_{model} = \sigma_{predicted}(1 + \theta \Delta\theta) \tag{3}$$

$\Delta\theta$ is defined as the measured uncertainty of the ATLAS data in a given transverse momentum bin, while θ is the nuisance parameter that can be varied in the model.

The likelihood is maximised using an algorithm called Minuit2, which automatically varies the parameters until to determine the shape of the fit until the all parameters are increasing. For parameters with limits, they are transformed using inverse trigonometric functions so that the transformed parameters can vary without limits James and Winkler [2004]. The fit uses a 'shape-only' fit that excludes the normalisation factor for the cross-section, that would otherwise add a constraint to the coupling modifiers in the fit.

We can construct the likelihood ratio out of the conditional and unconditional maximum likelihoods. The conditional likelihood is defined as the likelihood function where all parameters are freely floating except for κ_c, while the unconditional likelihood also sets κ_c to be freely floating. Then, the likelihood ratio is constructed in the Equation 4 Collaboration [2022]:

$$\Lambda(k_c) = \frac{L_{conditional}(\hat{\vec{\kappa}}, \hat{\vec{\theta}} | \kappa_c = k_c)}{L_{unconditional}(\hat{\vec{\kappa}}, \hat{\vec{\theta}})} \tag{4}$$

After this, a test statistic can be made using the Equation 5 below. Test statistics determine whether to accept or reject the null hypothesis, so that each value of the test statistic corresponds to a specific confidence ratio.

$$T = -2 \ln \Lambda(k_c) \tag{5}$$

On the following page, Figure 8, Figure 9 and Figure 10 are some graphs called 'Negative Logarithm Likelihood' scans. Taking 20 values of k_c, and then plotting them on the x-axis, versus the test statistic T on the y-axis, will produce a curve that will intersect with lines corresponding to 68% and 95% confidence levels. For κ_c and κ_b they are [-9.8, 11.5] and [-2.0, 8.1] for 68% confidence limit respectively. For the 95% confidence limit, they are [-14.4, 18.9] and [-3.7, 10.2] respectively. These confidence intervals will be further constrained when normalisation is taken into account.

To test a simpler parameterisation where the production modes independent of κ_c, κ_b and κ_t are merged, the cross-sections for them are combined. These production modes are independent of all Yukawa couplings, as they only involve interactions between Vector bosons V, i.e. the W^-, W^+ and Z bosons. They can be merged by adding the cross-sections of each channel directly. For uncertainties, they are statistical variances that are assumed to be independent, so they must be summed using the quadrature formula as given in Equation 6 for the uncertainties given for each bin in each channel. The overall effect of the merging procedure is to weaken the constraints on the parameters by a small amount. For instance, the 95% confidence limits for κ_c became [-14.5, 18.8] while for κ_b, they became [-3.8, 10.3].

$$\Delta x = \sqrt{(\Delta x_1)^2 + (\Delta x_2)^2 + \ldots + (\Delta x_n)^2} \tag{6}$$

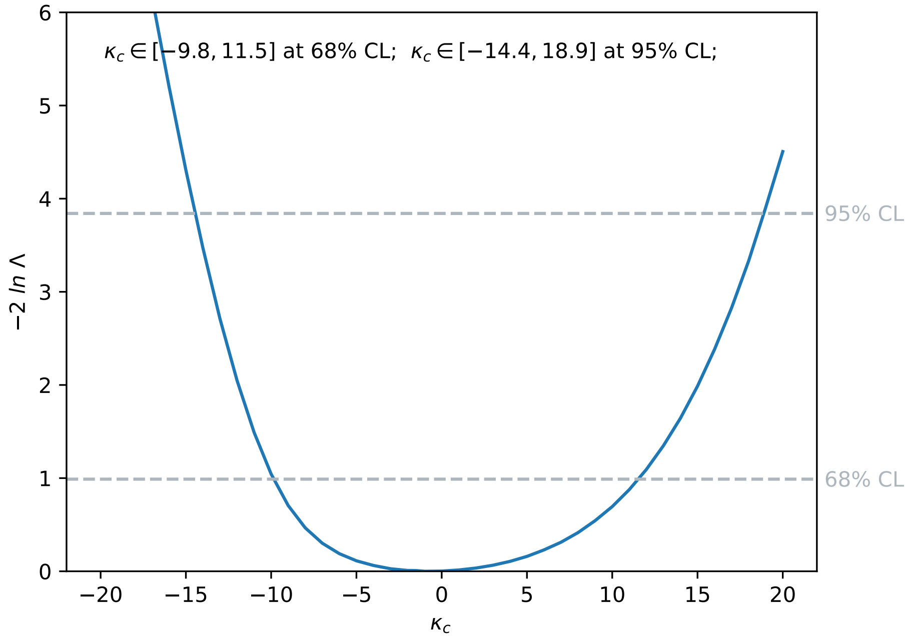

Figure 8: The κ_c NLL scan. There are actually 2 minimums but they overlap.

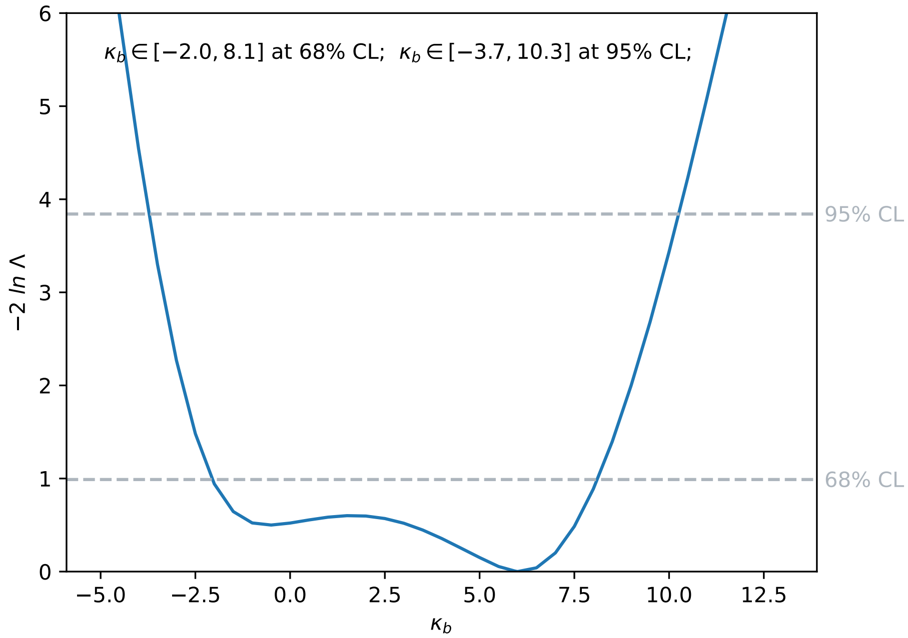

Figure 9: The κ_b NLL scan. There are 2 minimums as the model is quadratic in κ_b.

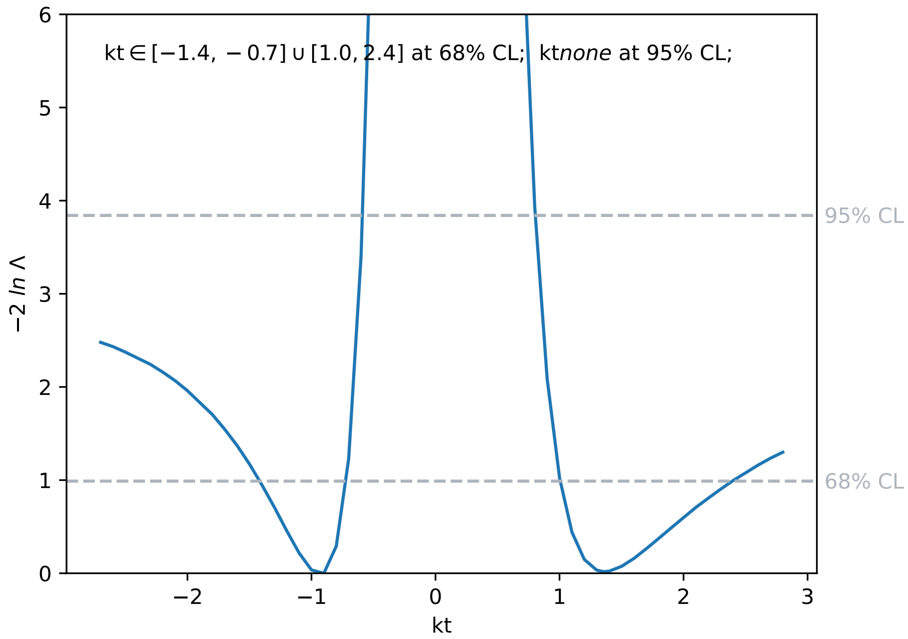

Figure 10: The κ_t NLL scan. the minimums are completely separate and diverge as the cross-sections for the Top-Yukawa interaction dominate, and are also significantly more constrained due to this.

The parameterisation of the model only included κ_c and κ_b at first, and κ_t was fixed at the Standard Model value. But it could be incorporated into the parameterised model and turned into a freely floating parameter so that another Negative-Log Likelihood scan could be performed.

Impact ranking plots are used to evaluate the robustness of the merging process. They vary the nuisance parameters while the κ_b and κ_c are freely floated Collaboration [2023b]. The impact ranking plots are shown in Figures 11 and 12, for unmerged and merged parameterisationsrespectively. They contain 2 sets of information, the pulls and the effects on κ_b. The pulls are shown in terms of deviations from the mean nuisance parameter and they show the constraints on the nuisance parameters in the model. The effects on κ_b are measured in terms of the standard deviation of maximum Likelihood value of κ_b as the nuisance parameters are varied.

For the merged and unmerged parameterisations, the impact ranking plot can visualise whether merging the uncertainties worked properly. For example, the impacts of the nuisance parameter $theta_merged_qcd$ is significantly larger than the unmerged $theta_QCD$ nuisance parameters, and it is spread between negative and positive impacts on κ_b, unlike the positive-only impact on κ_b that the unmerged $theta_QCD$ parameters display. This is explained by the unmerged nuisance parameters being squared in Equation 6, which means that the signs of the uncertainty are lost. Otherwise, the merging process appears to work well for this nuisance parameter.

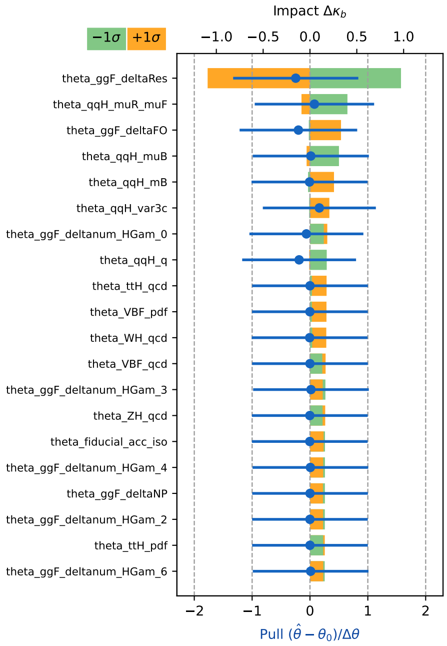

Figure 11: Impact Rankings for κ_b, unmerged channels

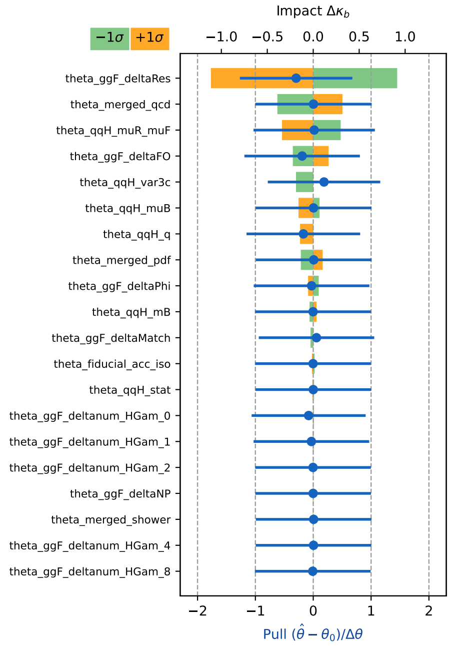

Figure 12: Impact Rankings for κ_b, merged channels

Expected results for Natural-log Likelihood scans can be constructed using Asimov data. This is a Gaussian-distributed toy dataset which is designed to use the covariance matrix of the ATLAS measurements with the mean of the Asimov data being the predicted cross-section Cowan et al. [2011]. This essentially assumes that a background-only hypothesis, where in this case the background is the Standard Model predictions. It can give the expected constraints on $kappa_c$, $kappa_b$ and $kappa_t$ if the Standard Model value of these couplings is assumed to be true. The expected results are shown in Figures 13, 14, and 15.

Due to the measurement uncertainties and the fiducial volume of the ATLAS detector, the Negative-Log Likelihood scans for Asimov data have intrinsically have tighter constraints for κ_c, κ_b and κ_a than their counterparts using which use the real ATLAS data. However, confidence intervals of the Asimov Negative-Log Likelihood scans fit within those of the real Negative-Log Likelihood scans, which indicates that the observed data is compatible with the predicted data.

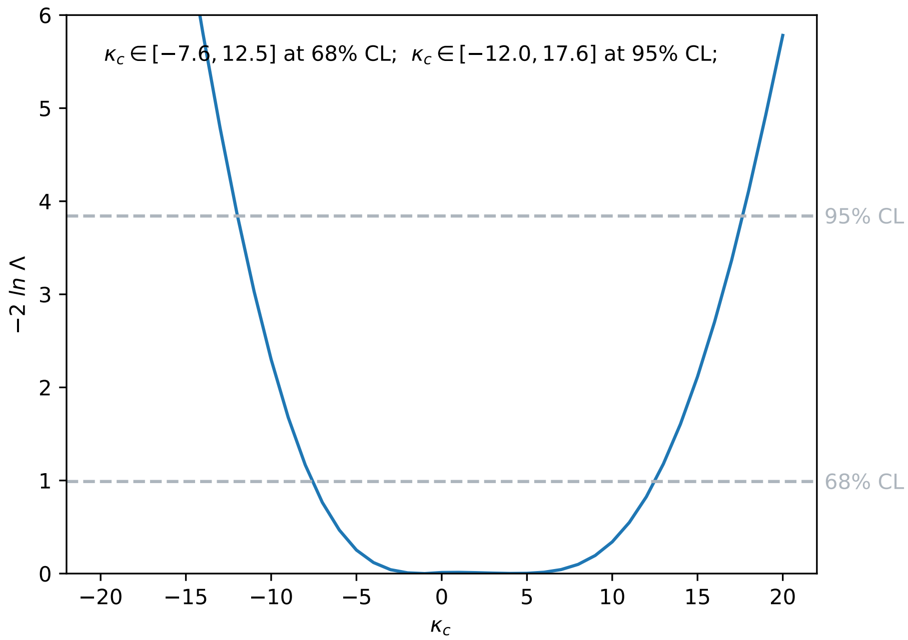

Figure 13: Negative-Log Likelihood scan for κ_b using Asimov data.

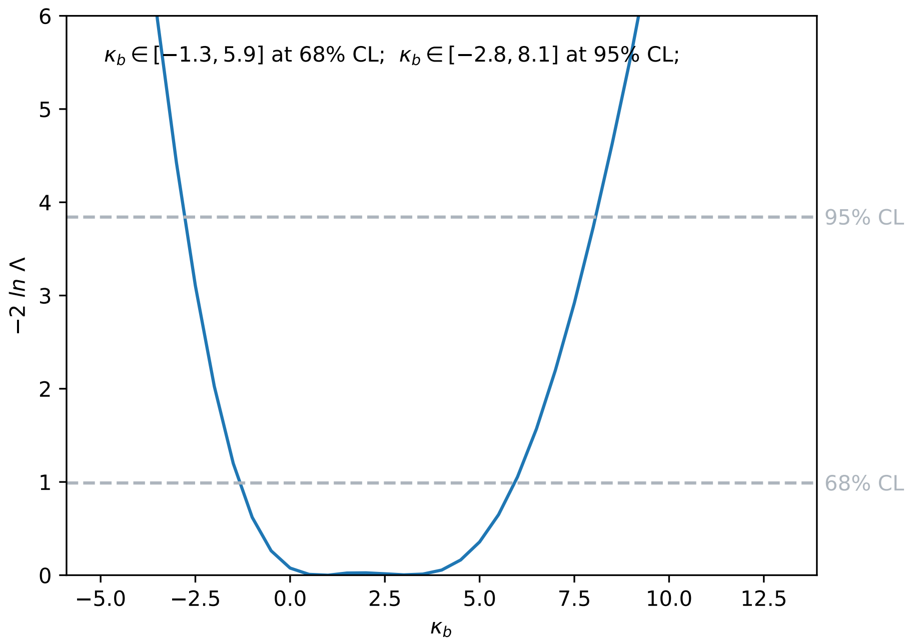

Figure 14: Negative-Log Likelihood scan for κ_b using Asimov data. Notice that there are 2 tiny minima right next to each other, because these minima are a relic of the quadratic terms in the parameterised model.

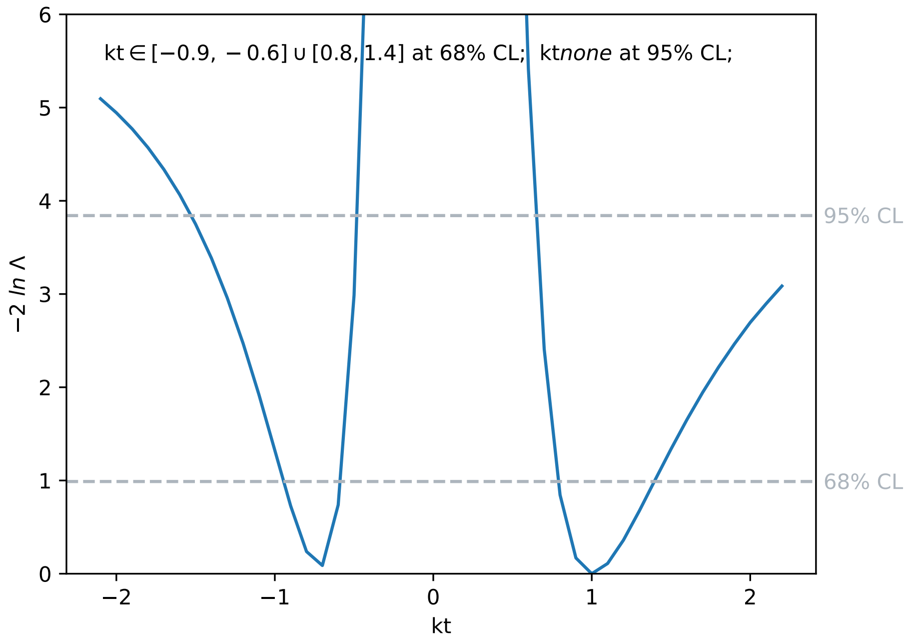

Figure 15: Negative-Log Likelihood scan for κ_t using Asimov data. Because the measured data for κ_t has a stronger constraint than the others and is known to be close to 1, that's why the minimum is around 1.

4 Conclusions

Charm-Yukawa interaction is an intriguing area of investigation because there is the potential for the coupling modifier to deviate from the Standard Model. Currently, the direct $H \to c\bar{c}$ decay has been measured to constrain the Charm-Yukawa coupling modifier even better than the indirect method that is being investigated in this paper, however it is possible to combine the two constraints to make an even stronger constraint.

In future we hope to create a 3-dimensional graph of both κ_b and κ_c with respect to the test statistic, as hopefully this could allow us to see potential correlations between the bottom and charm quark couplings. In addition, we want to integrate the systematic uncertainties into the model as free parameters rather than fixing them to measured values.

References

Riccardo Maria Bianchi and ATLAS Collaboration. ATLAS experiment schematic or layout illustration. General Photo, 2022. URL https://cds.cern.ch/record/2837191.

The ATLAS Collaboration. A detailed map of higgs boson interactions by the atlas experiment ten years after the discovery. *Nature*, 607(7917):52–59, July 2022. ISSN 1476-4687. doi: 10.1038/s41586-022-04893-w. URL http://dx.doi.org/10.1038/s41586-022-04893-w.

Henric Wilkens and (on behalf ofthe ATLAS LArg Collaboration). The atlas liquid argon calorimeter: An overview. *Journal of Physics: Conference Series*, 160(1):012043, apr 2009. doi: 10.1088/1742-6596/160/1/012043. URL https://dx.doi.org/10.1088/1742-6596/160/1/012043.

The ATLAS Collaboration. Measurement of the higgs boson mass with $h \to \gamma\gamma$ decays in $140fb$ of $\sqrt{s} = 13$ tev pp collisions with the atlas detector. *Physics Letters B*, 847: 138315, December 2023a. ISSN 0370-2693. doi: 10.1016/j.physletb.2023.138315. URL http://dx.doi.org/10.1016/j.physletb.2023.138315.

ATLAS. Measurements of W H and Z H Higgs production with decays into bottom quarks and direct constraints on the charm Yukawa coupling with 13 TeV collisions in the ATLAS detector. Technical report, CERN, Geneva, 2024. URL https://cds.cern.ch/record/2905263. All figures including auxiliary figures are available at https://atlas.web.cern.ch/Atlas/GROUPS/PHYSICS/CONFNOTES/ATLAS-CONF-2024-010.

Petar Bokan, Laurelle Maria Veloce, Haider Abidi, Chiara Arcangeletti, Andrea Gabrielli, Paolo Francavilla, Nicolas Morange, Kerstin Tackmann, Sarah Heim, Frued Erik Braren, Gangcheng Lu, Giovanni Marchiori, Daniela Kuchler, Kurt Brendlinger, Nils Gillwald, Martina Laura Ojeda, Roberto Di Nardo, Hongtao Yang, Ahmed Tarek, Marko Stamenkovic, Miha Muskinja, Tao Wang, Yusheng Wu, Heather Gray, and Tristan Arnoldus Du Pree. Combination of the total inclusive and differential Higgs boson cross-sections and interpretations. Technical report, CERN, Geneva, 2022. URL https://cds.cern.ch/record/2804361.

CMS Collaboration and ATLAS Collaboration. Combination of measurements of the top quark mass from data collected by the atlas and cms experiments at $\sqrt{s} = 7$ and 8 tev, 2024. URL https://arxiv.org/abs/2402.08713.

R. L. Workman et al. Review of Particle Physics. *PTEP*, 2022:083C01, 2022. doi: 10.1093/ptep/ptac097.

The ATLAS Collaboration. Measurement of the total and differential higgs boson production cross-sections at $\sqrt{s} = 13$ tev with the atlas detector by combining the$h \to zz* \to 4l$ and $h \to \gamma\gamma$ decay channels. *Journal of High Energy Physics*, 2023(5), May 2023b. ISSN 1029-8479. doi: 10.1007/jhep05(2023)028. URL http://dx.doi.org/10.1007/JHEP05(2023)028.

Fred James and Matthias Winkler. *MINUIT User's Guide*, 6 2004.

Glen Cowan, Kyle Cranmer, Eilam Gross, and Ofer Vitells. Asymptotic formulae for likelihood-based tests of new physics. *The European Physical Journal C*, 71(2), February 2011. ISSN 1434-6052. doi: 10.1140/epjc/s10052-011-1554-0. URL http://dx.doi.org/10.1140/epjc/s10052-011-1554-0.

The ATLAS Collaboration. Measurement of the total and differential higgs boson production cross-sections at

$$\sqrt{s}$$

= 13 tev with the atlas detector by combining the h → zz* → 4 and h → decay channels. *Journal of High Energy Physics*, 2023(5), May 2023c. ISSN 1029-8479. doi: 10.1007/jhep05(2023)028. URL http://dx.doi.org/10.1007/JHEP05(2023)028.